The Effect of Pt Particle Size on the Oxidation of CO, C3H6, and NO Over Pt/Al2O3 for Diesel Exhaust Aftertreatment

Hansen, Thomas Klint; Høj, Martin; Hansen, Brian Brun; Janssens, Ton V.W.; Jensen, Anker Degn

Published in:
Topics in Catalysis

Link to article, DOI:
10.1007/s11244-017-0818-9

Publication date:
2017

Document Version
Peer reviewed version

The Effect of Pt Particle Size on the Oxidation of CO, C_3H_6, and NO over Pt/Al_2O_3 for Diesel Exhaust Aftertreatment

Thomas Klint Hansen[1], Martin Høj[1], Brian Brun Hansen[1], Ton V.W. Janssens[2], Anker Degn Jensen[1]*

[1]Department of Chemical and Biochemical Engineering, Technical University of Denmark, Kgs. Lyngby, Denmark

[2]Haldor Topsøe A/S, Kgs. Lyngby, Denmark

*Corresponding author: Anker Degn Jensen, aj@kt.dtu.dk

Abstract

Platinum-based oxidation catalysts applied for diesel exhaust aftertreatment constitute a significant part of system costs. Effective utilization of platinum is therefore relevant to reduce costs while retaining performance. To this end, the influence of Pt particle size on catalytic activity for CO, hydrocarbon, and NO oxidation was studied. 1 wt.% Pt/Al_2O_3 catalysts were prepared by wet impregnation, drying, and different calcination and thermal treatments, yielding Pt particles with diameters between 1.3 and 18.7 nm, as determined by CO pulse titration and transmission electron microscopy. Activity measurements for CO, C_3H_6, and NO oxidation showed an optimal Pt particle size with respect to the mass based activity between 2-4 nm for all three reactions. From measured turnover frequencies and site statistics of Pt particles, the reactions appear to be mainly catalyzed by terrace atoms, which are most abundant between 2-4 nm. The decrease in catalytic activity for large Pt particles is therefore due to the diminishing Pt surface area, while the decrease in activity for small particles is due to the lack of terrace atoms required for CO, HC, and NO oxidation.

1. Introduction

In order to comply with strict emission control regulations [1, 2], modern diesel-driven vehicles are equipped with a catalytic exhaust aftertreatment system to reduce the emission of harmful compounds [3]. The main harmful compounds in a diesel exhaust gas are particulate matter (soot particles), NO_x, CO, and unburnt hydrocarbons (HC), which are converted to CO_2, H_2O, and N_2 in the aftertreatment system [3]. To achieve this, a modern aftertreatment system typically consists of a diesel oxidation catalyst (DOC), a diesel particulate filter (DPF) and a catalytic NO_x abatement unit further downstream, which consists of a catalyst for the selective catalytic reduction with NH_3 (NH_3-SCR) combined with an ammonia slip catalyst (ASC) for oxidation of residual NH_3 (see Figure 1).

Figure 1.

The temperature in the exhaust gas varies, depending on the driving load, but generally lies in the range 200-500°C [3-5]. The combination of a high exhaust gas flow (500-1500 m^3/h) [4] and a limited space for catalysts requires a good catalyst performance at high space velocities while maintaining a low pressure drop at any operating temperature. This is achieved by using catalysts coated on monolith substrates [6]. Furthermore, diesel fuel contains sulfur compounds that when combusted lead to SO_x in the exhaust gas, which can poison and deactivate catalysts during operation [5, 7].

The main purpose of the DPF is to capture the soot particles produced in the engine. A common type of filter is the wall-flow filter, in which the exhaust gas is forced through the walls of a monolith, whereby the soot particles are retained [3, 5]. The amount of soot accumulated in the filter increases with time, which results in

an undesired pressure drop. Therefore, some regeneration of the filter is required. One method to do this is active regeneration, which entails periodically raising the temperature to above 600°C by injection of post engine fuel, which causes the soot to burn in the oxygen of the exhaust gas [3, 5]. An alternative method is passive regeneration, in which the temperature for soot oxidation is lowered to the normal operating temperature range (350-500°C), which makes a continuous soot oxidation under normal operation possible. To this end, a catalyst for soot oxidation can be applied to the DPF, or NO_2 generated in the DOC can be used for the removal of soot [3, 5].

The NO_x abatement system consists of a catalyst for the selective catalytic reduction with NH_3 (NH_3-SCR) combined with an ammonia slip catalyst (ASC) [3]. In the SCR reactions, NO_x is converted by ammonia and oxygen to N_2 and H_2O, with high selectivity [3, 5, 8]. The ammonia is usually provided by injection of urea at the inlet to the SCR unit. In practice, a 5-10% excess of ammonia is used in the NH_3-SCR to improve the performance [8], and the ASC removes the excess ammonia by selective oxidation of ammonia with oxygen to N_2 and water [9]. The presence of NO_2, up to a NO_2/NO_x ratio of 0.5, can also improve the SCR performance, as it allows for the fast-SCR reaction to occur [5, 8].

The DOC removes CO and unburnt hydrocarbons in the exhaust gas by oxidation to CO_2 and H_2O. Additionally, the DOC is used to oxidize NO to NO_2, which, as mentioned above, may improve SCR performance and enhance the regeneration of the DPF in systems using passive regeneration [3, 5, 7]. DOC formulations are usually based on Pt supported on metal oxides [5, 7]. Pt is also less sensitive to sulfur, compared to other noble metals and metal oxides [5, 7], making the catalysts robust in environments with small amounts of SO_2 and SO_3. To improve the thermal stability of the DOC and reduce cost, some of the Pt can be replaced by Pd, although Pd is significantly less tolerant to sulfur [5, 7].

The support materials used in a DOC are common metal oxides, such as Al_2O_3, SiO_2, CeO_2, TiO_2, ZrO_2, zeolites, or a combination of these [5]. A common support material is γ-Al_2O_3, due to its high surface area (100-200 m^2/g) and good thermal stability [5]. Therefore, Pt/Al_2O_3 is a good model catalyst for a DOC, and has been used in many studies on Pt catalysts [5, 10-45].

A focus area for DOC development is the improvement of low temperature catalytic activity [5, 10, 46]. This is relevant due to the development of more fuel-efficient engines, which result in lower exhaust gas temperatures. In addition, a good low temperature activity also helps reduce the emissions during cold start of the engine, which account for a significant part of the total emissions [3, 4].

Another development of the DOC is aimed at cost reduction, either by replacement of the noble metal with cheaper materials or by a more effective use of the noble metals, allowing for a significant reduction of the noble metal content [5, 11, 46]. High catalytic activity and cost-effective utilization of metals is generally associated with small particles (high dispersion) of the active phase [5, 12, 13]. However, small Pt particles show a low turnover frequency (TOF) for CO oxidation [12, 47, 48], HC oxidation [13-18], and NO oxidation [12, 19, 20] in studies with a large excess of oxygen relative to reactants, similar to conditions in diesel exhaust aftertreatment, e.g. 10 vol.% O_2, 5 vol.% H_2O, 1000 ppm NO_x, 300 ppm HC, 1000 ppm CO [49]. As a result, an optimum in Pt particle size exists, with a corresponding maximum in catalytic activity.

To our knowledge, no studies investigate the influence of Pt particle size on the oxidation of CO, HC, and NO, relevant for the diesel oxidation catalyst, over the same catalysts. Furthermore, few studies include H_2O in the feed gas, which is present in diesel exhaust gas (2-12 vol.% H_2O) and promotes CO oxidation while inhibiting both HC and NO oxidation [7, 21-23]. It was therefore the purpose of this work to investigate the effect of Pt particle size for all three oxidation reactions relevant for the DOC (CO, HC, and NO) under diesel exhaust gas conditions, and identify the respective optimal Pt particle sizes over a broad range of average Pt particle

diameters (between 1.3-18.7 nm). The feed gas for activity measurements contained either 2.8 or 7.8 vol.% water vapor and about 10 vol.% O_2 in order to better emulate the catalytic activity under diesel exhaust gas conditions. We show that the oxidation of CO, C_3H_6, and NO all exhibit the same optimum Pt particle size range and that the high mass based catalytic activity does not necessarily coincide with the maximum TOF. We relate these observations to the change in abundance of corner, edge, and terrace atoms.

2. Experimental

2.1 Catalyst Preparation

To prepare Pt/Al_2O_3 catalysts with different Pt particle sizes, two batches of alumina were impregnated with 1 wt.% Pt and dried. The batches were then split into smaller portions before being calcined and thermally treated with different temperatures, gas atmospheres, and durations (see Table 1) in order to obtain a series of nine catalysts with different Pt particle sizes in the range 1.3 to 18.7 nm.

For the impregnations, 3 g or 10 g of γ-Al_2O_3 support material (Puralox NWa-155; Sasol; surface area 153.7 m^2/g) was suspended in an aqueous solution (20 mL solution/g γ-Al_2O_3) of 2.59 mM $H_2PtCl_6 \cdot 6H_2O$ (ACS reagent; Sigma-Aldrich) under stirring at 50°C in an open beaker [48]. The water evaporated overnight and a dry solid sample remained. The samples were dried further in a horizontal tube furnace (ETF 30-50/15-S; Entech) in 3 NL N_2/min at 80°C for 4 hrs. Subsequent calcination and thermal treatments were done in the same horizontal tube furnace. From the first batch of 3 g, two portions of 1 g each were given the oxidative calcination treatments (O_2/N_2 or $H_2O/O_2/N_2$) presented in Table 1, yielding samples A and B. The entire second batch of 10 g was calcined in a 3 NL/min flow of N_2 at 550°C for 8 hrs and a 1 g portion was taken as sample C. Six 1 g portions of the remaining batch were then exposed to the different thermal treatments presented in Table 1, yielding samples D to I. The use of a chlorine Pt precursor can lead to residual chlorine after calcination that can inhibit catalytic activity [50, 51], but the calcination and thermal treatments applied in this study, together

with the presence of H_2O in the reactor feed (Section 2.2.2), will effectively remove chlorine [50, 51]. Additionally, a commercial 1 wt.% Pt/Al_2O_3 powder catalyst (205966; Sigma-Aldrich) was used as a benchmark in both fresh, SA1, and thermally treated states, SA2. The properties and thermal treatment of the benchmark catalysts are also presented in Table 1. Table 1 presents an overview of the eleven catalysts studied, indicating their calcination and thermal treatments, as well as the resulting Pt dispersion and average Pt particle diameter calculated from the CO adsorption capacity and verified by TEM (Section 2.2.1).

Table 1.

The Pt contents of samples A, D, and SA1 were determined by inductively coupled plasma optical emission spectrometry (ICP-OES), and were assumed to be representative of each respective batch. The Pt contents of the three batches were very similar with 0.94 wt.% Pt for the first batch (samples A and B), 0.98 wt.% Pt for the second batch (samples C to I), and 0.92 wt.% Pt for the commercial catalyst (samples SA1 and SA2). These Pt contents were used for subsequent calculations. The eleven catalyst samples were tableted, crushed, and sieved to a fraction of 150-300 µm before further characterization and testing.

2.2 Catalyst Characterization

2.2.1 Pt Particle Size

The catalysts were analyzed by CO pulse titration (Autosorb-iQ_2; Quantachrome Instruments) to measure CO adsorption capacity, which was used to calculate the Pt dispersion and average Pt particle diameter. The procedure for pretreatment and CO pulse titration was as follows: First, a 0.5 g sample was heated to 100°C (10°C/min) and dried in a 30 NmL/min flow of air for 30 minutes. To remove impurities, the sample was then heated to 350°C (10°C/min) and oxidized in a 30 NmL/min flow of air for 30 minutes. Next, the system was

evacuated and the sample cooled to 100°C under vacuum. A 30 NmL/min flow of pure H_2 was then introduced and the sample was heated to 350°C (10°C/min) and reduced for 120 minutes. The system was then evacuated and the sample was heated to 550°C (10°C/min) under vacuum and held at 550°C for 120 minutes to remove any adsorbed water formed from the oxidative and reductive treatments. After cooling to 35°C under vacuum, CO pulse titration was performed at 35°C using a 279 µL injection loop filled with pure CO and a 30 NmL/min flow of He carrier gas. A thermal conductivity detector (TCD) at the sample cell outlet measured the CO in the effluent gas and was used to determine the CO adsorption capacity ($N_{CO\ ads}$; mmol CO_{ads}/g_{Pt}). After CO pulse titration, the sample was heated to 550°C (20°C/min) in a 30 NmL/min flow of He to desorb CO from the catalyst surface and then cooled to room temperature. For most samples, the characterization was repeated for a second portion of the catalyst sample and the average of the two measurements was used. Analyzed samples were subsequently stored at room temperature in ambient air.

Assuming that CO adsorbs as a monolayer on the Pt surface atoms, the CO adsorption capacity is directly proportional to the number of surface Pt atoms ($N_{Pt,S}$; Pt_S atom/g_{Pt}). Using a stoichiometric factor of unity for the adsorption of CO on Pt [42, 52, 53], the Pt dispersion (D_{Pt}; %) is calculated as the ratio of surface Pt atoms to the total number of Pt atoms (N_{Pt}; Pt atom/g_{Pt}):

$$D_{Pt} = \frac{N_{Pt,S}}{N_{Pt}} \cdot 100\% = \frac{N_{CO\ ads}}{N_{Pt}} \cdot 100\% \quad (1)$$

Note that for equation (1), the units of $N_{CO\ ads}$ are simply number of CO molecules/g_{Pt}. The surface-averaged Pt particle diameter (d_{Pt}; nm) is calculated from the ratio of Pt volume (V_{Pt}; $Å^3$ Pt/g_{Pt}) to Pt surface area ($A_{Pt,S}$; $Å^2$ Pt/g_{Pt}), assuming hemispherical Pt particles [52]. The Pt volume is calculated from the Pt density (ρ_{Pt}; $2.145 \cdot 10^{-23}$ $g_{Pt}/Å^3$ Pt [53]), while the Pt surface area is calculated from $N_{Pt,S}$ and the cross-sectional area of one Pt atom ($A_{Pt,X}$; 8.0 $Å^2$ Pt/Pt atom [53]). The equation for the average Pt particle diameter is therefore:

$$d_{Pt} = 6 \cdot \frac{V_{Pt}}{A_{Pt,S}} = \frac{6}{\rho_{Pt} \cdot N_{Pt,S} \cdot A_{Pt,X}} \quad (2)$$

Catalyst samples C, D, and I were analyzed using Transmission Electron Microscopy (TEM) to verify the average Pt particle diameters determined from CO pulse titration. A FEI Titan ETEM, running at a 300 kV acceleration voltage with spherical aberration corrector was used to characterize the samples in vacuum at room temperature. The Pt particles observed had a close to circular shape and the Pt particle diameters were therefore measured for a circle that tightly outlined each particle.

2.2.2 Activity Measurements

The catalysts were tested for the oxidation of CO, HC, and NO. All samples used in the activity measurements were taken from the portion previously used in the CO pulse titration, and which had subsequently been stored at room temperature in ambient air (Section 2.2.1).

The CO oxidation activity was measured using a quartz U-tube reactor (D_i = 3 mm). The reactor was loaded with a mixture of 10 mg catalyst (150-300 µm) and 50 mg glass beads (212-300 µm), fixed between two plugs of quartz wool. The flow was directed upwards through the catalyst bed, and the temperature was measured with a thermocouple placed inside the reactor at the catalyst bed outlet.

To measure the CO oxidation activity, a flow of a 310 NmL/min was used with a feed gas consisting of 240 ppm CO, 2.8 vol. % H_2O, 9.7 vol. % O_2, and balance N_2, resulting in a space velocity of 0.021 mol/(g_{cat}·s). Water vapor was added to the gas mixture by bubbling it through a heated water flask at 30°C. The activity measurements were done by heating the catalyst from 40°C to 550°C at a rate of 5°C/min, holding at 550°C for 1 hour, followed by cooling to about 40°C. The cooling rate was set to 5°C/min, which could be followed until about 425°C where the cooling rate became limited to the natural cooling of the system. The concentrations of CO and CO_2 in the gas were measured using a continuous gas analyzer (Uras-26; ABB) and the concentration of water was determined using a humidity probe (HC2-IC102; Rotronic), which were both placed after the reactor.

The heating and cooling procedures were repeated on the same reactor loading in most cases, to check repeatability of the results.

The catalysts were tested for hydrocarbon oxidation in the same manner as described above for CO oxidation, by replacing CO with 145 ppm of propene. Even though a typical diesel exhaust contains a variety of hydrocarbon components, propene (C_3H_6) was used as a model compound for hydrocarbon oxidation, following common practice [5, 10, 11, 23, 24, 46]. The propene conversion was determined based on the CO_2 concentrations measured in the product gas, using the same analyzer as for CO oxidation, and the stoichiometry of the reaction equation, forming three CO_2 molecules per C_3H_6 molecule. The CO_2 concentrations measured at 550°C corresponded to full conversion and these were used to determine the feed concentration of propene, which agreed well with that expected from the set gas flows.

For NO oxidation, a different flow reactor setup equipped with a NO_x analyzer was used. A quartz U-tube reactor (D_i = 6 mm) was loaded with a mixture of 20 mg catalyst sample (150-300 µm) and 100 mg glass beads (212-300 µm), fixed between two plugs of quartz wool. The gas flowed upwards through the catalyst bed and the temperature was measured with a thermocouple placed inside the reactor at the catalyst bed outlet. The feed gas was 485 ppm NO, 7.8 vol. % H_2O, 9.7 vol. % O_2, and balance N_2, with a total flow of 1030 NmL/min, resulting in a space velocity of SV = 0.035 mol/(g_{cat}·s). Water was added to the gas mixture by bubbling a separate flow of N_2 through water at 80°C. The concentrations of NO and NO_2 were measured using a continuous gas analyzer (Limas11-HW; ABB) and the concentration of water was determined using a humidity probe (HC2-IC102; Rotronic). The procedure for the activity measurements were similar to those used in CO and C_3H_6 oxidation, with heating from 100°C to 550°C at a rate of 5°C/min, holding at 550°C for 1 hour, and cooling to 100 °C. The cooling was done at an initial rate of 5°C/min until the heat loss became controlling at 450°C and the cooling rate became lower. For NO oxidation, heating and cooling procedures were repeated a

second and third time for two different catalysts, and these showed no significant difference (see Figure S4 in Supplementary Data). Therefore, the repeated cycles were omitted for all other samples in the measurement for NO oxidation.

3. Results

3.1 Determination of Pt Particle Size

Table 1 presents the CO adsorption capacity measured by CO pulse titration for the different catalysts, as well as the calculated Pt dispersions and average Pt particle diameters. Since Pt dispersion and Pt particle diameter are inversely proportional, we choose to use the Pt particle diameter to describe the dispersion and to obtain a direct reference to the Pt particle size. The data in Table 1 shows that the calcination atmosphere and subsequent thermal treatments with various temperatures, gas atmospheres, and durations can be used to vary the average Pt particle diameter of the catalyst.

The smallest Pt particles were obtained for samples A, B, and C that were only calcined at 550°C for 8 hrs, with different gas atmospheres during calcination having a limited effect. Calcination in a wet oxidative atmosphere produced the smallest Pt particles of 1.3 nm (sample A) and the dry oxidative atmosphere yielded slightly larger Pt particles of 1.6 nm (sample B), while calcination in a dry inert atmosphere of N_2 resulted in a small additional increase to 2.1 nm (sample C). These results indicate that Pt particles of 1-2 nm are obtained from the initial calcination of $[PtCl_6]^{2-}$ adsorbed on the surface of γ-Al_2O_3 and can be controlled to some extent by varying the calcination atmosphere between pure N_2 and wet or dry oxidative atmospheres.

Pt particles larger than 2 nm were formed by thermally treating catalyst samples that had been prepared by calcination in a dry N_2 atmosphere at 550°C for 8 hrs, corresponding to sample C. The increase in Pt particle diameter was controlled by varying the temperatures, durations, and atmospheres of the thermal treatments.

Thermally treating the catalysts in a flow of N_2 at 600°C, 650°C, or 750°C for 12 hrs gave limited increases in Pt particle diameter for samples D (2.7 nm), E (3.0 nm), and F (3.2 nm) in Table 1. Furthermore, increasing the duration of the thermal treatment in a flow of N_2 at 750°C from 12 hrs (sample F) to 48 hrs (sample G) led to a slight increase in Pt particle diameter from 3.0 nm to 4.3 nm. To form the large Pt particles of samples H (7.7 nm) and I (18.7 nm), the thermal treatments of catalysts were done in a flow of N_2, O_2, and water vapor at 650°C or 750°C for 8 hrs. Similarly, the fresh Sigma-Aldrich catalyst with 2.1 nm Pt particles (sample SA1) was thermally treated in a flow of N_2, O_2, and water vapor at 550°C for 8 hrs, yielding sample SA2 with relatively larger Pt particles of 4.5 nm. Overall, these results indicate that the combination of oxygen, water vapor, and high temperature drives the sintering of Pt particles.

Figure 2 shows TEM images for catalyst samples C, D, and I, alongside the number based particle size distributions and the corresponding log-normal distributions. The Pt particles of sample C are mostly between 1-4 nm, with an average Pt particle diameter of 2.5 ± 1 nm, while most particles of sample D are between 1-4.5 nm with an average Pt particle diameter of 2.8 ± 1 nm. These Pt particle sizes match well with 2.1 and 2.7 nm found from CO pulse titration. For sample I, which has much larger particles, only 19 particles were identified by TEM. The sizes vary from 11-63 nm, but the majority of the particles are between 11 and 22 nm. This is also in good agreement with the results from CO pulse titration, with an estimated average particle size of 18.7 nm. These results indicate that the average Pt particle diameters obtained by CO pulse titration are a good estimate of the Pt particle size.

Figure 2.

3.2 Effect of Pt Particle Size on Activity

During the 1st heating cycle to 550°C, changes in the prepared catalysts occur leading to higher activity, while the data for the 1st cooling and 2nd heating/cooling cycles are comparable, indicating that the catalysts have reached a stable state after the initial heating to 550°C (see Figures S1, S2, S3, and S4 of the Supplementary Data). Sintering may occur during the 1st heating and cooling cycle, but the overlaying activity measurements of SA1 (2.1 nm) and SA2 (4.5 nm) for C_3H_6 oxidation (see Figure S2a and S2b), which unlike CO and NO oxidation does not exhibit hysteresis behavior [54], indicate that sintering is negligible for samples with Pt particles of 2.1 nm or larger. The samples with Pt particles smaller than 2.1 nm, such as A (1.3 nm) and B (1.6 nm), will still have the smallest Pt particles after the 1st heating and cooling cycle, and sintering will at most shift the particle sizes partly towards 2.1 nm. This gives a small margin of uncertainty in the exact Pt particle size of A and B used in the following presentation of results.

The activity measurements from the 1st cooling cycles for CO oxidation, C_3H_6 oxidation, and NO oxidation, are shown in Figure 3. All catalysts are active for each of the three oxidation reactions, but clear differences in the temperatures at which the rate of each reaction becomes appreciable are observed. For the most active catalysts, this occurs in the range of 45-65°C for CO oxidation, 100-130°C for C_3H_6 oxidation, and 150-250°C for NO oxidation.

Figure 3.

Figure 3a shows the CO conversion during the 1st cooling cycle. Above 120°C, the catalysts all maintain complete oxidation of CO to CO_2. For the catalysts with average particle diameters of 1.6 (B), 2.1 (C), 2.1 (SA1),

2.7 (D), and 3.2 nm (F), the CO oxidation starts at the lowest temperature and these are therefore the most active. The catalysts with smaller and larger particles all require a higher temperature for CO oxidation and are therefore less active, pointing to an optimal Pt particle size for CO oxidation. The oscillatory behavior seen for sample C (2.1 nm) in Figure 3a and for sample F (3.0 nm) in Figure S1c of the Supplementary Data, is known for CO oxidation over Pt and the phenomena associated with this have been thoroughly discussed elsewhere [25, 26, 55], and is beyond the scope of this article.

A similar trend is observed for C_3H_6 oxidation. In Figure 3b, the C_3H_6 conversion during the 1st cooling cycle shows that the onset temperature of the reaction is higher than for CO oxidation. Below 100°C, no significant C_3H_6 conversion is obtained for any catalyst and above 180°C full conversion of C_3H_6 is reached. The catalysts with Pt particles diameters of 2.1 (SA1), 2.7 (D), and 3.2 nm (F) were the most active, while smaller and larger Pt particles resulted in a lower catalytic activity, indicating an optimum in Pt particle size for C_3H_6 oxidation as well.

For NO oxidation, the data looks quite different compared to CO and C_3H_6 oxidation. Figure 3c shows the NO conversion during the 1st cooling cycle with a maximum in conversion between 325-450°C. This maximum is due to the NO_2 decomposition imposed by the thermodynamic equilibrium of the reaction NO + ½ O_2 ↔ NO_2, which shifts toward NO + O_2 with increasing temperature, resulting in a lower NO conversion at higher temperatures. The equilibrium NO conversion is indicated by the dashed black line in Figure 3c. Below 300°C, where the contribution of the reverse reaction is limited, there are significant differences in catalytic activity observed. The most active catalysts have an average Pt particle diameter of 2.1 (SA1), 2.7 (D), 3.0 (E), and 4.3 nm (G). This indicates that there is an optimal particle size for NO oxidation, like for CO and C_3H_6 oxidation.

In order to better visualize the observed trends of activity with the Pt particle diameter, we used the temperature at which 50% conversion was measured (T_{50}) for CO oxidation and C_3H_6 oxidation. For NO

277 oxidation, not all catalyst samples reached 50% conversion and therefore, the temperature for 20% conversion
278 (T_{20}) was used instead. A lower T_{50} or T_{20} corresponds to a higher activity; the choice of conversion level is
279 arbitrary and different choices did not lead to significantly different trends. Figure 4 shows the observed trends
280 for the T_{50} and T_{20} with the Pt particle size, derived from 1st cooling and 2nd heating/cooling cycles for CO, C_3H_6,
281 and NO oxidation. In Figure 4, for catalysts with repeated CO pulse titration measurements, the end points of
282 the error bars indicate the individual Pt particle sizes calculated from the repetitions.

283

284 **Figure 4.**

285

286 For CO oxidation, in Figure 4a, the catalysts with an average Pt particle diameter of 1.6 (B), 2.1 (C), 2.1 (SA1),
287 2.7 (D), and 3.2 nm (F) show the lowest T_{50} at around 60 °C, and therefore are the most active catalysts for CO
288 oxidation. The T_{50} for smaller particles is about 75°C for 1.3 nm (A) and about 110 °C for very large particles of
289 18.7 nm (I), indicating a significantly lower activity for these catalysts. A similar trend is observed for C_3H_6
290 oxidation in Figure 4b; catalysts with an average Pt particle diameter of 2.1 (SA1), 2.7 (D), and 3.2 nm (F)
291 achieve the lowest T_{50} of about 135°C. The T_{50} for both the smallest particles of 1.3 nm (A) and largest of 18.7
292 nm (I) are about 148°C. For NO oxidation, in Figure 4c, the T_{20} is lowest for samples with Pt particle diameters
293 of 2.1 (SA1), 2.7 (D), 3.0 (E), and 4.3 nm (G) at about 220°C. The largest Pt particles of 18.7 nm (I) show an
294 increase in T_{20} to 275°C, related to a decrease in activity. In contrast, decreasing the Pt particle diameter to 1.3
295 nm (A) results in a very significant increase of T_{20} to 380°C and therefore a significant decrease in the catalytic
296 activity. These data show that the highest activity for all three reactions relevant for application of Pt as diesel
297 oxidation catalyst is obtained for catalysts with an average Pt particle diameter in the range of 2-4 nm.

298 To check whether the loss of activity for larger particles is due to the loss of Pt surface area, the turnover
299 frequency (TOF = mol/(s·mmol Pt_s)) was determined for the CO, C_3H_6, and NO oxidation reactions. If the loss of
300 surface area solely causes the loss of activity for larger Pt particles, then the TOF should remain constant. The
301 TOF was calculated from the mass based rate of reaction (r'= mol/(s·g_{Pt})) and the number of surface Pt atoms,
302 $N_{Pt,S}$ per gram platinum, as derived from the CO adsorption capacity, $N_{CO\ ads}$. The rate of reaction rate, r', was
303 evaluated for each reaction at the temperature at which 10% conversion was reached for the most active
304 catalyst, to ensure differential conditions. The TOF was therefore evaluated at 50°C for CO oxidation (10% CO
305 conversion for sample D (2.7 nm)), at 105°C for C_3H_6 oxidation (10% conversion for sample F (3.2 nm)), and
306 190°C for NO oxidation (10% conversion for sample SA1 (2.1 nm)).

307 The TOFs for CO, C_3H_6, and NO as function of average Pt particle diameter are presented in Figure 5 along with
308 the rates of reaction and CO adsorption capacities. From Figure 5a, the TOF for CO oxidation increases from 1.3
309 (A) to 2.7 nm (D), achieving the maximum TOF value for 2.7 nm (D). An increase in the Pt particle diameter to
310 4.5 (SA2) and 18.7 nm (I) causes a steep decrease in the TOF for CO oxidation. Furthermore, the maximum in
311 rate of reaction for CO oxidation coincides with the maximum TOF at a Pt particle size of 2.7 nm (D). For the
312 C_3H_6 oxidation TOF in Figure 5b, the TOF increases with the Pt particle diameter from 1.3 (A) to 3.2 nm (F). For
313 larger Pt particles, the TOF continues to increase slightly, unlike the TOF for CO oxidation. Although the highest
314 C_3H_6 TOF value is observed for 18.7 nm (I) Pt particles, the maximum mass based rate of reaction is measured
315 for the samples with a Pt particle size between 2-4 nm. Similarly, the TOF for NO oxidation in Figure 5c
316 increases with a change in the Pt particle diameter from 1.3 (A) to 2.1 (SA1) - 2.7 nm (D), and has significantly
317 higher values for 7.7 nm (H) and 18.7 nm (I). For C_3H_6 and NO oxidation, the maximum TOF does therefore not
318 correspond to the maximum in the mass based rate of reaction for 2-4 nm Pt particles. The fact that the TOF
319 for C_3H_6 and NO oxidation does not decrease significantly for large particles is consistent with a loss of activity
320 due to a decrease of Pt surface.

4. Discussion

An optimum in the rate of reaction for the oxidation of CO, C_3H_6, and NO was observed for Pt particle diameters of 2-4 nm for all three reactions. For application as a DOC, this means that tuning the Pt particle size to this range enhances the CO, HC (C_3H_6), and NO oxidation reactions. However, the TOF does not follow this trend. For CO oxidation, the maximum in TOF occurs for 2-3 nm Pt particles [12], while the TOF increases with Pt particle size for both HC oxidation [13-18] and NO oxidation [12, 19, 20]. The observation that the optimum particle diameter coincides with a maximum in TOF for CO oxidation but not for HC and NO oxidation indicates that the reasons for the maxima in rates of reaction are different.

A phenomenon occasionally used to explain particle size effects is the transition from a metallic to a non-metallic behavior that occurs when Pt particles become sufficiently small, since the band structure responsible for the metallic character of Pt cannot fully develop for very small particles [30, 31, 56, 57]. In general, this effect is most significant for clusters and particles below 1 nm in size for Pt/γ-Al_2O_3 [30, 57]. The smallest average Pt particle diameter considered in this work is 1.3 nm, and therefore we expect this effect to have a minor contribution to the lower TOF for the small Pt particles in this study. Instead we focus on the changes in the distribution of types of surface Pt atoms with variation in Pt particle sizes, and the resulting influence on catalyst behavior.

A change in Pt particle size affects the relative number of corner, edge, and terrace atoms, and since the contribution of these surface Pt atoms to the catalytic activity can be different, the catalytic activity becomes dependent on the Pt particle size. Figure 6 shows the calculated total and relative abundance of corner, edge, and terrace Pt atoms as a function of the Pt particle diameter for a 1 wt.% Pt loading, with the assumption that the Pt particles have a truncated octahedral shape and are supported on a (111)-plane. The calculations are done as outlined in the supplementary material of reference [58]. Figure 6a shows that Pt particles smaller

than 4 nm have an appreciable number of edge and corner atoms, and that the number of terrace atoms starts to decrease, while the large Pt particles are dominated by terrace atoms. A comparison of Figure 6a with Figures 5b and 5c indicate that the TOFs for C_3H_6 and NO oxidation follow the relative amount of Pt terrace atoms, and the highest C_3H_6 and NO TOFs are obtained for large Pt particles, as previously reported [5, 12-20]. As a consequence, the maximum rates for HC and NO oxidation coincide with the maximum total number of terrace atoms, which occurs in the range of 2-4 nm. The decrease in reaction rate for large particles is then due to a lower number of Pt atoms in terraces.

Figure 6.

In contrast to HC and NO oxidation, the oxidation of CO exhibits a maximum in TOF at 2.7 nm and very low TOF for large Pt particles. Particles of 2.7 nm in diameter have a high amount of edge atoms, but the maximum amount of edge atoms is found at about 1.5 nm. If CO oxidation were governed by edge sites alone, then we should have found the highest CO oxidation activity for catalyst B, with a particle size of 1.6 nm. This indicates that edges are not the only source of catalytic activity for CO oxidation, and the maximum in TOF occurring close to the maximum in terrace atoms points to a contribution of the terrace atoms as well. The reason for the lower CO-oxidation activity of large Pt atoms is then the lack of edge sites, rather than the loss of terrace sites as was the case for HC and NO oxidation.

From the discussion above, it follows that the role of the terrace sites in HC and NO oxidation is different compared to CO oxidation. The higher activity of the terraces for the oxidation of NO has been ascribed to a reaction of O_2 with vacancies on terraces nearly saturated with O* adatoms [19]. As terraces bind the oxygen

atoms weaker, the vacancies are easier to create on terraces, thus favoring the NO oxidation. For hydrocarbon oxidation, the weakly bound O* species on terrace atoms are needed for the removal of H atoms in hydrocarbon oxidation [18]. For CO oxidation, the presence of edge sites is important, and the CO oxidation occurs preferentially between oxygen chemisorbed to step sites and CO adsorbed to terrace atoms [59-62]. The CO oxidation reaction then becomes dependent on the presence of both terrace and edge sites.

An alternative explanation for the importance of edge sites in CO oxidation is the effect of water on the CO oxidation reaction. By using isotopically labeled oxygen, it was shown that water is actually the main source of the oxygen in CO_2 in the low temperature CO oxidation over Pd/Al_2O_3 in a wet feed gas [63]. This suggests that CO_2 is in fact formed from CO and water in a water gas shift reaction, rather than by an oxidation of CO with oxygen. Pt is also an efficient catalyst for water gas shift [64], and therefore the water gas shift reaction can also occur in CO oxidation under the wet conditions in a diesel exhaust gas. The water gas shift reaction requires dissociation of the water molecule to form adsorbed OH fragments, which then react with CO to form CO_2. DFT calculations indicate that this step is difficult on a Pt(111) surface and large particles, but becomes easier with decreasing Pt particle size due to an increase in edge and corner atoms [65, 66]. Furthermore, the enhanced O_2 dissociation on the edge sites may actually be beneficial for the dissociation of H_2O, since H_2O can readily react with O* in the presence of an extra H_2O to facilitate the formation of OH* ($H_2O^* + O^* + H_2O^* \rightarrow 2\ OH^* + H_2O^*$) [67-69]. The subsequent formation of COOH* from CO* and OH* occurs more easily on terrace atoms (0.56 eV activation energy on Pt(111)) compared to step atoms (1.4 eV activation energy on Pt(211)) [70], and the final step, in which CO_2 is formed, occurs readily through the transfer of H from COOH* to a neighboring OH*, forming H_2O [69]. This means that the reaction pathway depends on both the edge atoms - for the dissociation of O_2 and H_2O - and on the terrace atoms for formation of COOH* [67, 68], in agreement with our observation that the maximum rate of CO oxidation is observed for a particle size that lies between the sizes corresponding to the maximum amount of edge and terrace atoms. In HC and NO oxidation, a similar

reaction path with water does not exist, and consequently, water has an inhibitive effect on HC and NO oxidation [7, 21-23].

The lower activity for small Pt particles below 2 nm can also be understood from the site distribution shown in Figure 6. Small particles contain mostly edge and corner atoms, and the lack of terrace atoms, which are required for the CO, HC, and NO oxidation reactions, then results in the low activities. Figure 6 shows that particles smaller than 2 nm contain less terrace atoms, which is in good agreement with our observation that both the activity and TOF are lower for catalysts with Pt particle size below 2 nm. Furthermore, small Pt particles are also more easily oxidized than large particles [40, 41, 68, 71] and, consequently, the reduction of small Pt particles becomes harder. This is indicated by the 100-150 °C higher reduction temperature of oxidized Pt particles of 1.5 nm in size compared to for Pt particles of 4 nm [40, 71]. However, as oxygen always is present under the typical conditions in a DOC, it is difficult to distinguish whether the lower activity is the result from a change in chemistry due to oxide formation, or due to the loss of active sites, as both effects always will occur simultaneously.

According to the discussion above, the optimal Pt particle size of 2-4 nm for the oxidation of CO, C_3H_6, and NO over Pt/Al_2O_3 catalysts in the presence of water is mainly determined by the number of terrace sites. For the oxidation of C_3H_6 and NO, Pt particles larger than approximately 4 nm are less active due to the loss in surface area, but the TOF remains more or less constant. For CO oxidation, edge sites also play a role, and therefore the larger particles are less active due to the loss of edge sites, resulting in a lower TOF for large particles. The lower activity and TOF for the oxidation CO, C_3H_6 and NO for particles smaller than 2 nm can be understood by the lower amount of terrace sites in such particles, although the effects of a higher stability of Pt oxide in small particles are possible and indistinguishable.

5. Conclusion

The optimum Pt particle size for the oxidation of CO, C_3H_6, and NO was investigated through preparation, characterization, and activity measurements of a range of 1 wt.% Pt/Al_2O_3 catalysts. The catalysts were prepared by wet impregnation and different calcination and thermal treatments, in order to obtain a range of samples with Pt particles diameters of 1.3-18.7 nm, as determined from CO pulse titration and verified by TEM.

Comparison of catalytic activity as a function of temperature and Pt particle diameter showed that the greatest catalytic activities were achieved for Pt particle diameters between 2-4 nm for all three reactions. The results indicate that for C_3H_6 and NO oxidation, terrace surface atoms achieved the highest TOF values and were identified as the most active type of surface atoms, with the greatest abundance of terrace atoms corresponding to the optimum Pt particle diameter between 2-4 nm. With increasing Pt particle size, the rate of reaction decreases due to the significant decrease in Pt surface area relative to the slight increase in TOF.

For CO oxidation, the particle size dependency is more complex and a maximum in TOF was observed for 2.7 nm, suggesting that CO oxidation under diesel exhaust conditions is dependent on both terrace and edge atoms. The dependence of CO oxidation on both terrace and edge atoms results in an optimum TOF between 2-4 nm, since the absence of terraces in small particles or edges in large particles effectively decreases the reaction rate of the individual reactions.

Based on the results in this study, a diesel oxidation catalyst based on Pt/Al_2O_3 with Pt particles between 2 and 4 nm in diameter is optimal for CO, hydrocarbon, and NO oxidation in the presence of water.

6. Acknowledgements

427 The authors would like to thank Ian Joseph Allen (Technical University of Denmark) for catalyst characterization
428 with TEM and Henrik Teglborg (Technical University of Denmark) for assistance in catalyst preparation. The
429 financial support from Innovation Fund Denmark under grant number 103-2012-3 is gratefully acknowledged.

7. References

[1] EU (2011) OJEU 25.6.2011:1-168

[2] EPA (2001) Fed Reg 66:5002-5193

[3] Walker A (2016) Top Catal 59:695-707

[4] Jääskeläinen H (2011) DieselNet, www.dieselnet.com/tech/diesel_exh.php. [Accessed 09.08.2016]

[5] Russell A, Epling WS (2011) Catal Rev 53:337-423

[6] (1998) DieselNet, www.dieselnet.com/tech/cat_substrate.php. [Accessed 20.08.2016]

[7] Majewski WA (2012) DieselNet, www.dieselnet.com/tech/cat_doc.php. [Accessed 09.08.2016]

[8] Janssens T, Falsig H, Lundegaard L, Vennestrøm P, Rasmussen S, Moses P, Giordanino F, Borfecchia E, Lomachenko K, Lamberti C, Bordiga S, Godiksen A, Mossin S, Beato P (2015) ACS Catal 5:2832-2845

[9] Shrestha S, Harold M, Kamasamudram K, Kumar A, Olsson L, Leistner K (2016) Catal Today 267:130-144

[10] Hazlett M, Epling W (2016) Catal Today 267:157-166

[11] Wong A, Kyriakidou E, Toops T, Regalbuto J (2016) Catal Today 267:145-156

[12] Boubnov A, Dahl S, Johnson E, Molina A, Simonesen S, Cano SHFM, Lemus-Yeges L, Grunwaldt JD (2012) Appl Catal B-Environ 126:315-325

[13] Gololobov AM, Bekk IE, Bragina GO, Zaikovskii VI, Ayupov AB, Telegina NS, Bukhtiyarov VI, Stakheev AY (2009) Kinet Catal 50:830-836

[14] Garetto TF, Apesteguía CR (2000) Catal Today 62:189-199

[15] Otto K, Andino J, Parks C (1991) J Catal 131:243-251

[16] Carballo LM, Wolf EE (1978) J Catal 53:366-373

[17] Radic N, Grbic B, Terlecki-Baricevic A (2004) Appl Catal B-Environ 50:153-159

[18] García-Diéguez M, Chin Y, Iglesia E (2012) J Catal 285:260-272

[19] Weiss B, Iglesia E (2009) J Phys Chem C 113:13331-13340

[20] Smeltz AD, Delgass WN, Ribeiro FH (2010) Langmuir 26:16578-16588

[21] Mihai O, Fathali A, Auvray X, Olsson L (2014) Appl Catal B-Environ 160-161: 480-491

[22] Hauptmann W, Votsmeier M, Gieshoff J, Drochner A, Vogel H (2009) Appl Catal B-Environ 93:22-29

[23] Auvray X, Olsson L (2015) Appl Catal B-Environ 168: 342-352

[24] Abedi A, Luo J, Epling W (2013) Catal Today 207:220-226

[25] Gänzler A, Casapu M, Boubnov A, Müller O, Conrad S, Lichtenberg H,Frahm R, Grunwaldt JD (2015) J Catal 328:216-224

[26] Singh J, Nachtegaal M, Alayon E, Stçtzel J, van Bokhoven JA (2010) ChemCatChem 2:653-657

[27] Chin Y, Buda C, Neurock M, Iglesia E (2011) J Catal 283:10-24

[28] Olsson L, Fridell E (2002) J Catal 210:340-353

[29] Auvray X, Pingel T, Olsson E, Olsson L (2013) Appl Catal B-Environ 129:517-527

[30] Behafarid F, Ono L, Mostafa S, Croy J, Shafai G, Hong S, Rahman TS, Bareb S, Cuenya BR (2012) Phys Chem Chem Phys 14:11766–11779

[31] Beck IE, Bukhtiyarov VI, Pakharukov IY, Zaikovsky VI, Kriventsov VV, Parmon VN (2009) J Catal 268:60-67

[32] Putna E, Vohs J, Gorte R (1997) Surf Sci 391:1178-1182

[33] García-Diéguez M, Iglesia E (2013) J Catal 301: 198-209

[34] Altman E, Gorte R (1986) Surf Sci 172:71-80

[35] Altman E, Gorte R (1988) Surf Sci 195:392-402

[36] Altman E,Gorte R (1989) J Phys Chem 93:1993-1997

[37] Singh J, van Bokhoven JA (2010) Catal Today 155:199-205

[38] Alayon E, Singh J, Nachtegaal M, Harfouche M, van Bokhoven JA (2009) J Catal 263:228-238

[39] Stakheev A, Batkin A, Teleguina N, Bragina G, Zaikovsky V, Prosvirin I, Kudorozhkov A, Bukhtiyarov V (2013) Top Catal 56:306-310

[40] McCabe R, Wong C, Woo H (1988) J Catal 114:354-367

[41] Wang C, Yeh C (2001) Appl Catal A-Gen 209:1-9

[42] Karakaya C, Deutschmann O (2012) Appl Catal A-Gen 445-446:221-230

[43] Matsuhashi H, Nishiyama S, Miura H, Eguchi K, Hasegawa K, Iizuka Y, Igarashi A, Katada N, Kobayashi J, Kubota T, Mori T, Nakai K, Okazaki N, Sugioka M, Umeki T, Yazawa Y, Lu D (2004) Appl Catal A-Gen 272:329-338

[44] Chan D, Tischer S, Heck J, Diehm C, Deutschmann O (2014) Appl Catal B-Environ 156-157: 153-165

[45] Allian A, Takanabe K, Fujdala K, Hao X, Truex T, Cai J, Buda C, Neurock M, Iglesia E (2011) J. Am. Chem. Soc 133:4498-4517

[46] Binder A, Toops T, Unocic R, Parks J, Dai S (2015) Angew Chem 127:13461-13465

[47] Gracia F, Bollmann L, Wolf E, Miller J, Kropf A (2003) J Catal 220:382-391

[48] Bamwenda GR, Tsubota S, Nakamura T, Haruta M (1997) Catal Lett 44:83-87

[49] (2010) DieselNet, www.dieselnet.com/tech/emi_gas.php. [Accessed 22.08.2016]

[50] Marceau E, Che M, Saint-Just J, Tatibouët JM (1996) Catal Today 29:415-419

[51] Marceau E, Lauron-Pernot H, Che M (2001) J Catal 197:394-405

[52] Lowell S, Shields J, Thomas M, Thommes M (2004) Chemisorption: Site Specific Gas Adsorption. In: Characterization of Porous Solids and Powders: Surface Area, Pore Size, and Density. Academic Publishers, pp 213-233

[53] Quantachrome Instruments (2015) Autosorb iQ and ASiQwin Gas Sorption System Operating Manual. Boynton Beach

[54] Abedi A, Hayes R, Votsmeier M, Epling WS (2012) Catal Lett 142:930-935

[55] Ertl G (2010) Reactions at Solid Surfaces. John Wiley & Sons, Inc.

[56] Prashar AK, Mayadevi S, Rajamohanan PR, Devi RN (2011) Appl Catal A-Gen 403:91-97

[57] Cuenya BR, Behafarid F (2015) Surf Sci Rep 70:135-187

[58] Carlsson A, Puig-Molina A, Janssens T (2006) J Phys Chem B 110:5286-5293

[59] Xu J, Henriksen P, Yates J (1992) J Chem Phys 97:5250-5252

[60] Yates J (1995) J Vac Sci Technol 13:1359

[61] Wang J, Li W, Borg M, Gustafson J, Mikkelsen A, Pedersen T, Lundgren E, Weissenrieder J, Klikovits J, Schmid M, Hammer B, Andersen J (2005) Phys Rev Lett 95:1-4

[62] Li W (2008) J Phys: Cond Matt 20:1-7

[63] Caporali R, Chansai S, Burch R, Delgado J, Hardacre AGC, Mantarosie L, Thompsett D (2014) Appl Catal B-Environ 147:764-769

[64] Boisen A, Janssens TVW, Schumacher N, Chorkendorff I, Dahl S (2010) J Mol Catal A Chem 315:163-170

[65] Bruix A, Rodriguez J, Ramírez P, Senanayake S, Evans J, Park J, Stacchiola D, Liu P, Hrbek J, Illas F (2012) J Am Chem Soc 134:8968-8974

[66] Fajín JLC, Cordeiro MNDS, Gomes JRB (2014) J Phys Chem A 118:5832-5840

[67] van der Niet MJTC, den Dunnen A, Juurlink LBF, Koper MTM (2010) J Chem Phys 132:174705

[68] Ono L, Croy J, Heinrich H, Cuenya B (2011) J Phys Chem C 115:16856-16866

[69] Gong X, Hu P, Raval R (2003) J Chem Phys 119:6324-6334

[70] Yoo J, Abild-Pedersen F, Nørskov J, Studt F (2014) ACS Catal 4:1226-1233

[71] Smrinov M, Kalinkin A, Vovk E, Bukhtiyarov V (2015) Kinet Catal 56:801-809

431

Figure 1: Diagram of a typical diesel exhaust aftertreatment system consisting of a diesel oxidation catalyst (DOC), a diesel particulate filter (DPF), the injection of urea or NH_3, a catalyst for the selective catalytic reduction of NO_x with NH_3 (NH_3-SCR), and an ammonia slip catalyst (ASC).

Table 1: Overview of catalysts prepared. Catalysts from the first batch (A-B) were given oxidative calcinations at 550°C for 8 hours, and no further thermal treatment. Catalysts from the second batch (C-I) were all initially calcined in a flow of N_2 at 550°C for 8 hours, and most samples (D-I) were subsequently given thermal treatments with different temperatures, atmospheres, and durations. 1 wt.% Pt/Al_2O_3 catalysts from Sigma-Aldrich, fresh (SA1) or thermally treated (SA2), were also considered. The atmospheres for calcination and thermal treatments were pure N_2, 10 vol.% O_2 in N_2, or 3 vol.% H_2O and 10 vol.% O_2 in N_2. The CO adsorption capacity, Pt dispersion, and average Pt particle size were determined by CO pulse titration. Average Pt particle diameters determined with TEM for samples C, D, and I are given in parentheses.

Figure 2: Left column: TEM images for samples C, D, and I. Right column: Number based Pt particle size distributions based on TEM images and corresponding log-normal distributions for samples C, D and I. μ is the number average Pt particle diameter with a standard deviation of σ.

Figure 3: Conversion curves for 1st cooling cycles. a) CO oxidation: 10 mg catalyst, 310 NmL/min gas flow, SV = 0.021 mol/(g_{cat}·s), 240 ppm CO, 2.8 vol.% H_2O, 9.7 vol.% O_2, and balance N_2. b) C_3H_6 oxidation: 10 mg catalyst, 310 NmL/min gas flow, SV = 0.021 mol/(g_{cat}·s), 145 ppm C_3H_6, 2.8 vol.% H_2O, 9.7 vol.% O_2, and balance N_2. c) NO oxidation: 20 mg catalyst, 1030 NmL/min gas flow, SV = 0.035 mol/(g_{cat}·s), 485 ppm NO, 7.8 vol.% H_2O, 9.7 vol.% O_2, and balance N_2. The dashed black line is the thermodynamic equilibrium for NO and NO_2.

Figure 4: Temperatures for 50% conversion (T_{50}) for 1 wt.% Pt/Al_2O_3 with varying Pt particle diameters during a) CO oxidation: 10 mg catalyst, 310 NmL/min gas flow, SV = 0.021 mol/(g_{cat}·s), 240 ppm CO, 2.8 vol.% H_2O, 9.7 vol.% O_2, and balance N_2, and b) C_3H_6 oxidation: 10 mg catalyst, 310 NmL/min gas flow, SV = 0.021 mol/(g_{cat}·s), 145 ppm C_3H_6, 2.8 vol.% H_2O, 9.7 vol.% O_2, and balance N_2. c) Temperatures for 20% conversion (T_{20}) for NO oxidation: 20 mg catalyst, 1030 NmL/min gas flow, SV = 0.035 mol/(g_{cat}·s), 485 ppm NO, 7.8 vol.% H_2O, 9.7 vol.% O_2, and balance N_2. The end points of the error bars indicate the individual Pt particle sizes for catalysts with repeated CO pulse titration measurements. For all three graphs, the black lines are to help guide the eye.

Figure 5: The turnover frequency (TOF, red) for varying Pt particle diameters calculated for a) CO oxidation at 50°C, b) C_3H_6 oxidation at 105°C, and c) NO oxidation at 190°C from the rate of reaction (r', blue) and CO adsorption capacity ($N_{CO\ ads}$, green), which is directly proportional to the number of available Pt atoms. The measurements are for the 1st cooling cycle. Solid lines for rate of reaction (r', blue) and turnover frequency (TOF, red) are to help guide the eye.

Figure 6: Calculated total and relative number of corner, edge and terrace atoms for Pt particles of different sizes, assuming a truncated octahedron geometry and perfectly uniform particle size distributions. Bottom panel: The total number of different Pt atoms per gram Pt (mmol Pt atoms/g_{Pt}). Top panel: The relative number of corner, edge, and terrace Pt atoms per specific Pt particle size, given as a percentage.

472 **Figure 1.**

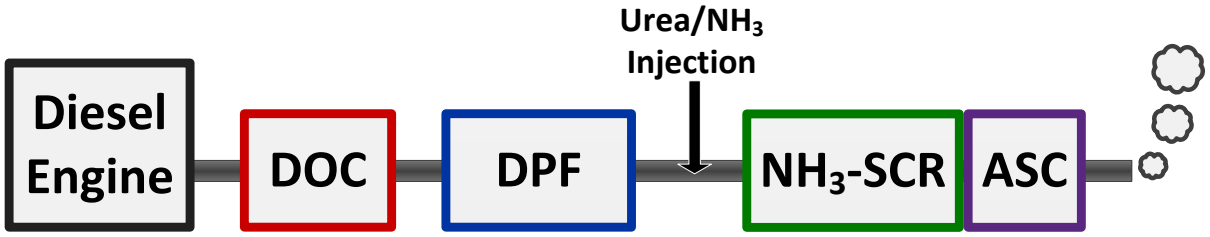

473

Table 1.

Sample Name	Calcination Atmosphere @550°C for 8 hrs	Thermal Treatment Temperature (°C)	Thermal Treatment Atmosphere ()	Thermal Treatment Duration (hrs)	CO Adsorption Capacity, $N_{CO\ ads}$ (mmol CO_{ads}/g_{Pt})	D_{Pt}, Pt Dispersion (%)	d_{Pt}, Average Pt Particle Diameter (nm)
A	$H_2O+O_2+N_2$	-	-	-	4.12	80	1.3
B	O_2+N_2	-	-	-	3.53	69	1.6
C	N_2	-	-	-	2.67	52	2.1 (2.5 ± 1)
D	N_2	600	N_2	12	2.13	42	2.7 (2.8 ± 1)
E	N_2	650	N_2	12	1.88	37	3.0
F	N_2	750	N_2	12	1.81	35	3.2
G	N_2	750	N_2	48	1.34	26	4.3
H	N_2	650	$H_2O+O_2+N_2$	8	0.74	14	7.7
I	N_2	750	$H_2O+O_2+N_2$	8	0.31	6	18.7 (23 ± 14)
SA1	Sigma-Aldrich	-	-	-	2.55	50	2.1
SA2	Sigma-Aldrich	550	$H_2O+O_2+N_2$	8	1.18	23	4.5

476 **Figure 2.**

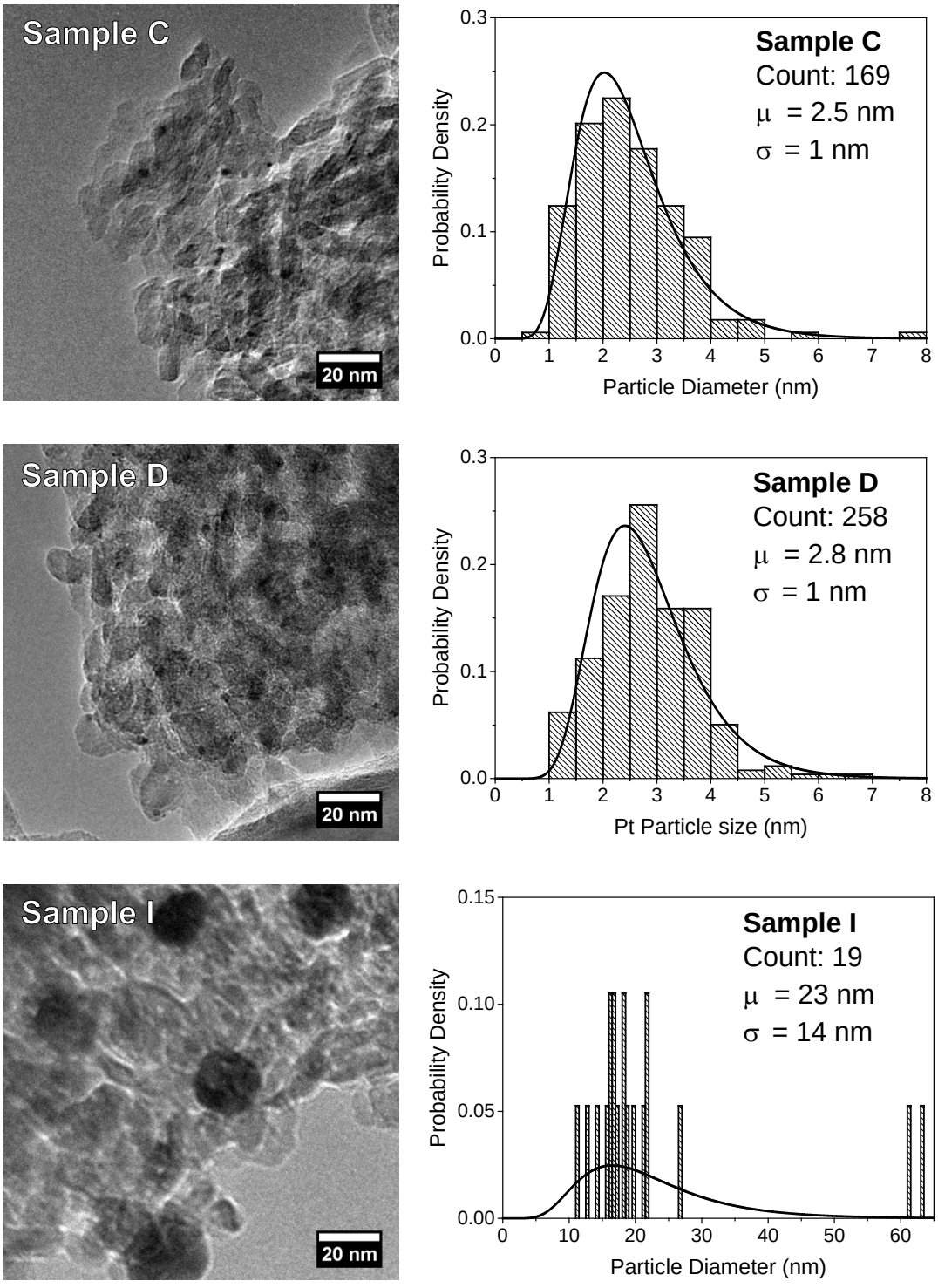

477

478 **Figure 3.**

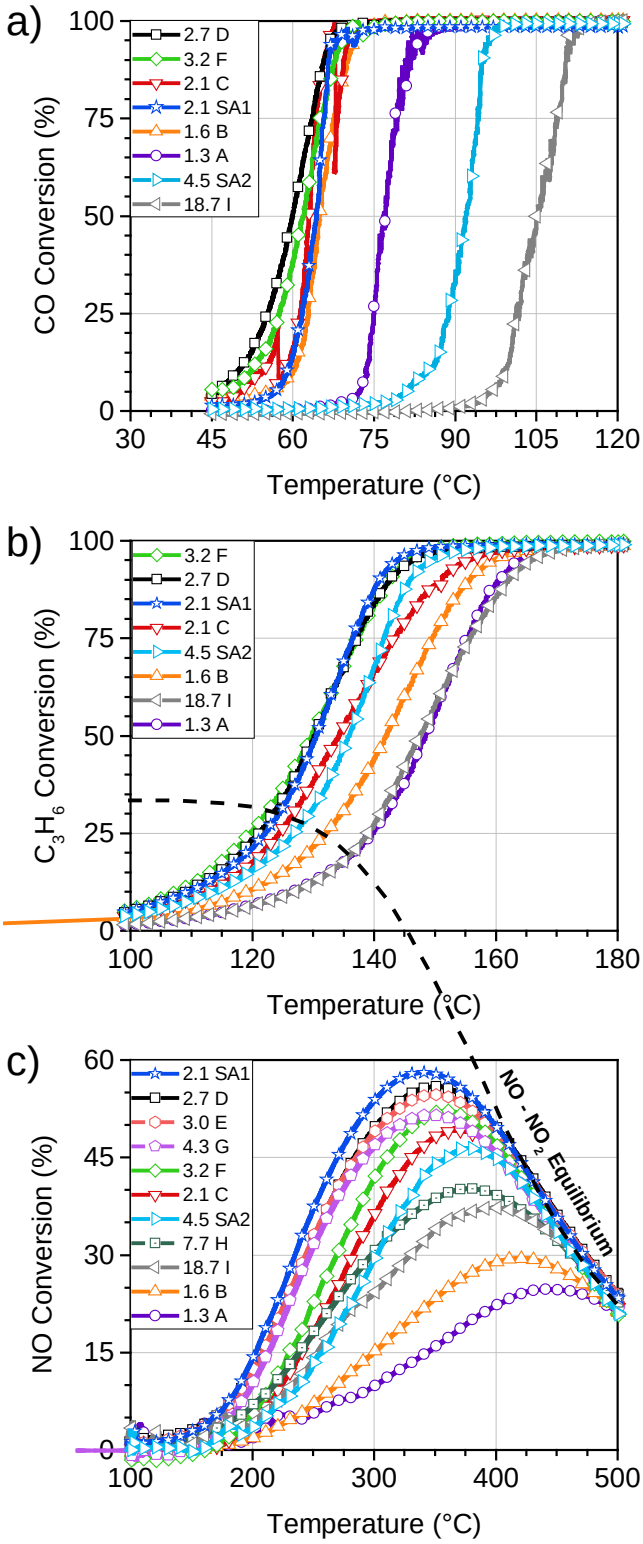

479

480 **Figure 4.**

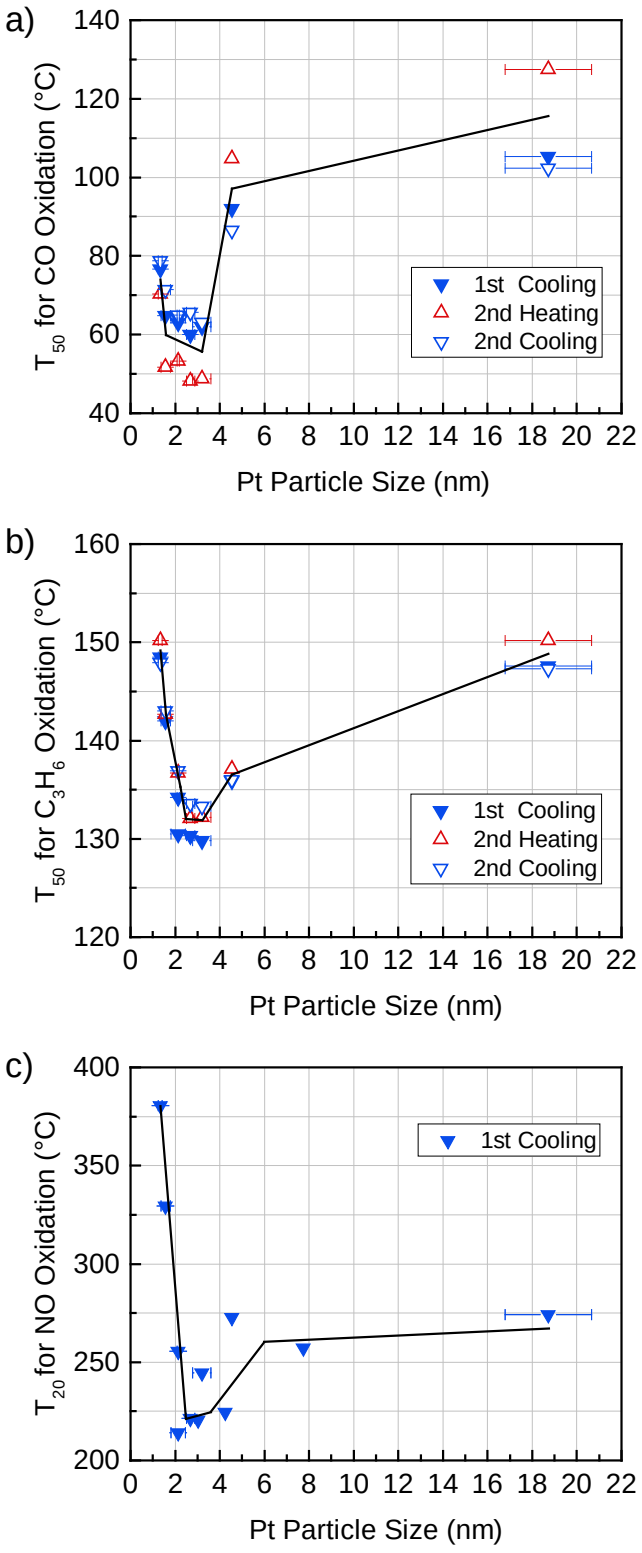

481

482 **Figure 5.**

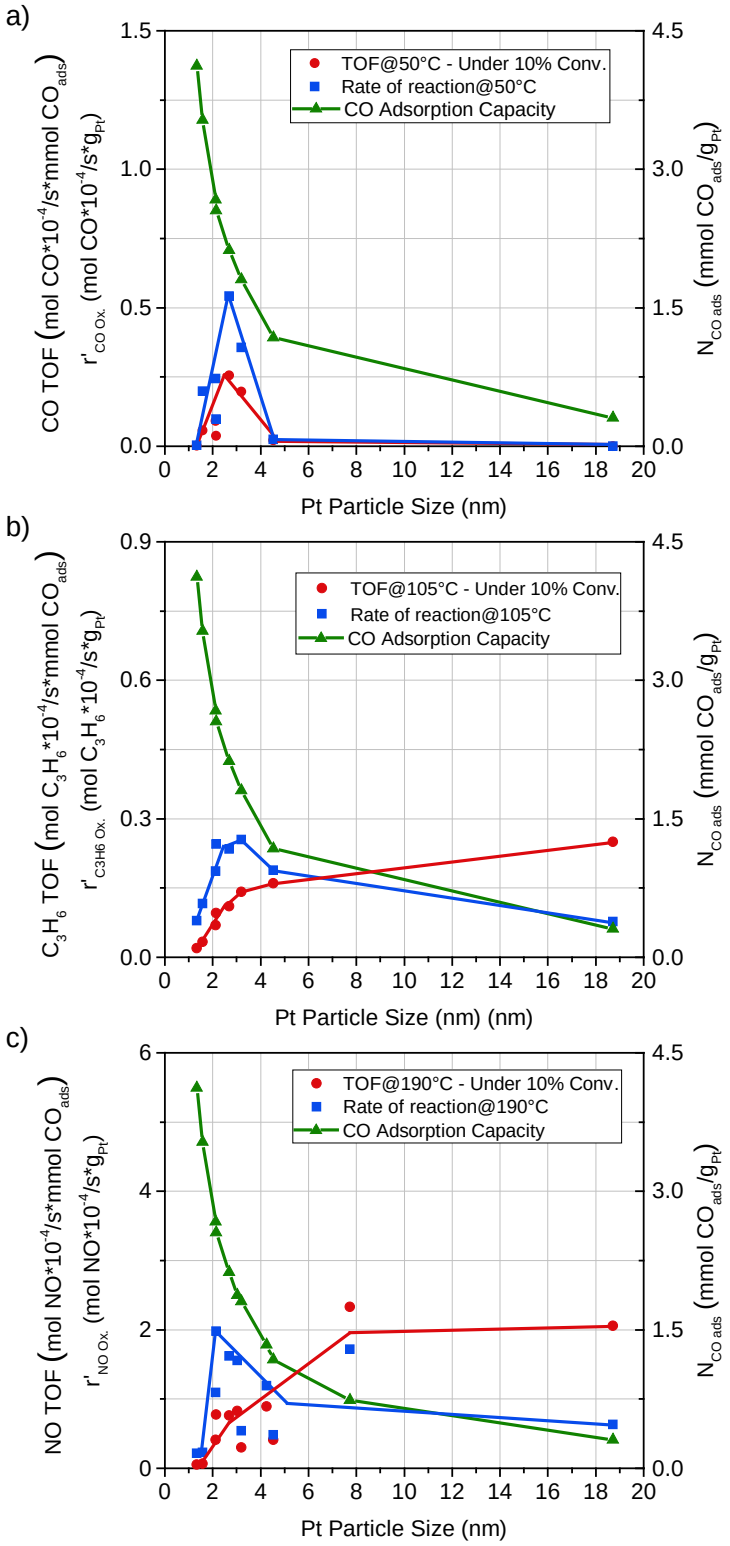

483

484 **Figure 6.**

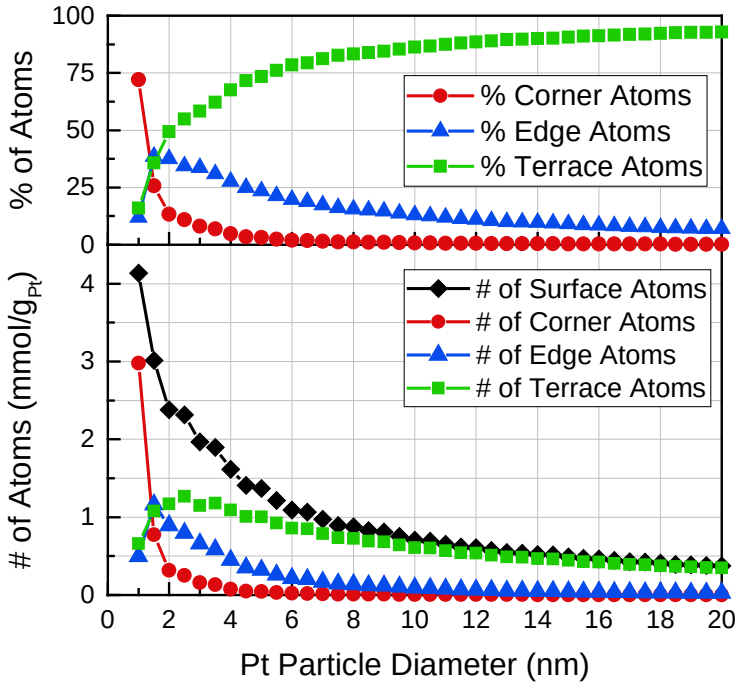

485

The Effect of Pt Particle Size on the Oxidation of CO, C_3H_6, and NO over Pt/Al_2O_3 for Diesel Exhaust Aftertreatment

Thomas Klint Hansen[1], Martin Høj[1], Brian Brun Hansen[1], Ton V.W. Janssens[2], Anker Degn Jensen[1]*

[1]Department of Chemical and Biochemical Engineering, Technical University of Denmark, Kgs. Lyngby, Denmark

[2]Haldor Topsøe A/S, Kgs. Lyngby, Denmark

*Corresponding author: Anker Degn Jensen, aj@kt.dtu.dk

A.1 Supplementary Data

Figures S1 and S2 show the activity measurements for CO and C_3H_6 oxidation over the 1 wt.% Pt/Al_2O_3 catalysts with varying Pt particle size for the a) 1st heating cycle, b) 1st cooling cycle, c) 2nd heating cycle, and d) 2nd cooling cycle. The activity measurements during the 1st heating cycle behave significantly different compared to the subsequent cooling and heating phases. This suggests that the catalysts undergo a change during the heating cycle shown in Figure S1a and Figure S2a, and that the catalysts reach a stable state after the initial heating to 550°C, indicated by the subsequently similar CO conversion curves.

Figure S1

Figure S2

Figure S3 shows the NO oxidation activity measurements for the a) 1st heating cycle and the b) 1st cooling cycle. Similarly to CO and C_3H_6 oxidation, the 1st heating curve for NO oxidation is significantly different than the subsequent cooling curve, indicating again a change in the catalyst.

Figure S3.

For NO oxidation, we decided to exhibit two different catalyst samples to repeated heating and cooling cycles in order to verify the stability of the catalysts tested. Figure S4 shows repeated heating and cooling cycles for 1 wt.% Pt/Al_2O_3 catalysts with an average Pt particle diameter of a) 1.3 nm (tested with four heating and cooling cycles) and b) 2.7 nm (tested with three heating and cooling cycles). The catalysts were prepared using the methods described in Section 2.1, with 1.3 nm Pt particles prepared using the same procedure as for sample A, while the sample with 2.7 nm Pt particles used the same procedure as for sample C, but with a calcination temperature of 750°C and a duration of 12 hours. Figure S4 shows again the significant change in catalytic activity from the 1st heating cycle to the subsequent cooling and heating cycles, for both samples. The subsequent cooling and heating cycles show a stable catalytic activity, with only limited changes occurring between the cooling cycles. Based on this we chose to limit the NO oxidation activity measurements to one heating and cooling cycle and used the activity measurement during the 1st cooling curve to compare catalytic activity of samples.

Figure S1: CO oxidation conversion curves for the a) 1st heating cycle, b) 1st cooling cycle, c) 2nd heating cycle, and d) 2nd cooling cycle. Operating conditions: 10 mg catalyst (150-300 µm), 50 mg inert glass beads (212-300 µm), 310 NmL/min gas flow, SV = 0.021 mol/(g_{cat}·s), 240 ppm CO, 2.8 vol.% H_2O, 9.7 vol.% O_2, and balance N_2.

Figure S2: C_3H_6 oxidation conversion curves for the a) 1st heating cycle, b) 1st cooling cycle, c) 2nd heating cycle, and d) 2nd cooling cycle. Operating conditions: 10 mg catalyst (150-300 µm), 50 mg inert glass beads (212-300 µm), 310 NmL/min gas flow, SV = 0.021 mol/(g_{cat}·s), 145 ppm C_3H_6, 2.8 vol.% H_2O, 9.7 vol.% O_2, and balance N_2.

Figure S3: NO oxidation conversion over 1 wt.% Pt/Al_2O_3 with for a) 1st heating cycle and b) 1st cooling cycle. Operating conditions: 20 mg catalyst (150-300 µm), 100 mg inert glass beads (212-300 µm), 1030 NmL/min gas flow, SV = 0.035 mol/(g_{cat}·s), 485 ppm NO, 7.8 vol.% H_2O, 9.7 vol.% O_2, and balance N_2.

Figure S4: NO oxidation conversions over 1 wt.% Pt/Al_2O_3 for several heating and cooling cycles with average Pt particle diameters of a) 1.3 nm and b) 2.7 nm. Operating conditions: 20 mg catalyst (150-300 µm), 100 mg inert glass beads (212-300 µm), 1030 NmL/min gas flow, SV = 0.035 mol/(g_{cat}·s), 485 ppm NO, 7.8 vol.% H_2O, 9.7 vol.% O_2, and balance N_2.

Figure S1.

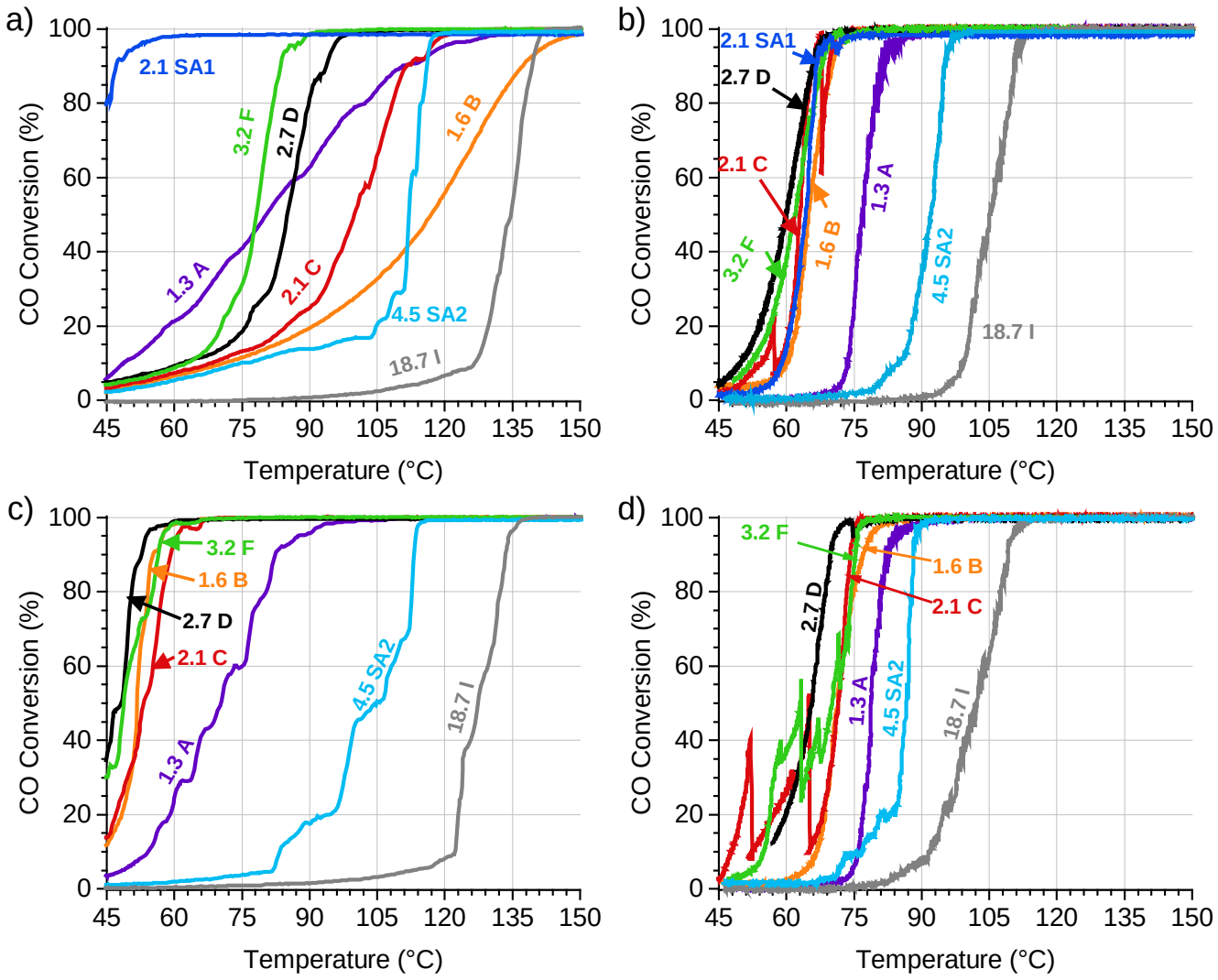
a)
b)
c)
d)
CO Conversion (%)
Temperature (°C)
2.1 SA1
3.2 F
2.7 D
1.6 B
1.3 A
2.1 C
4.5 SA2
18.7 I

543 **Figure S2.**

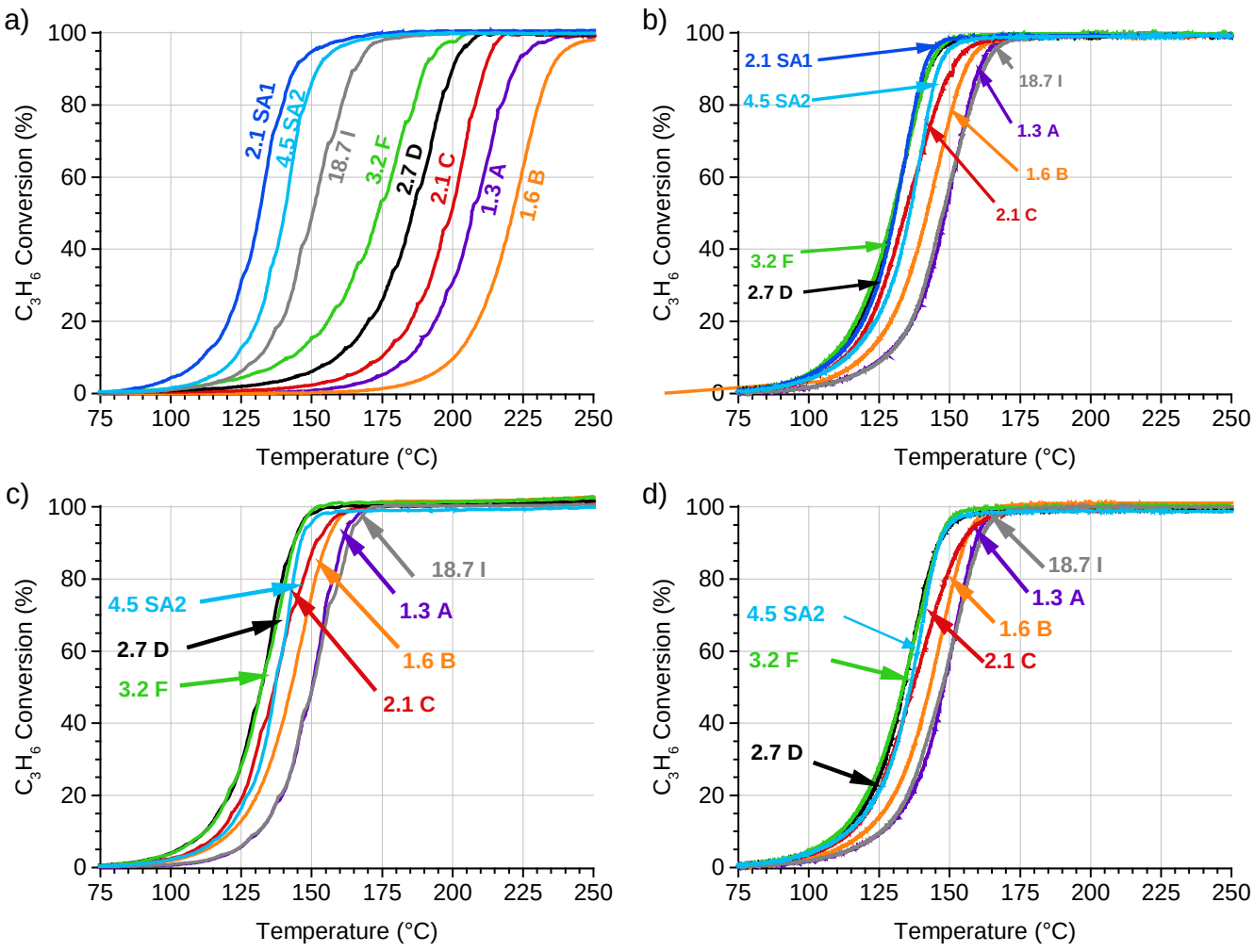

544

Figure S3.

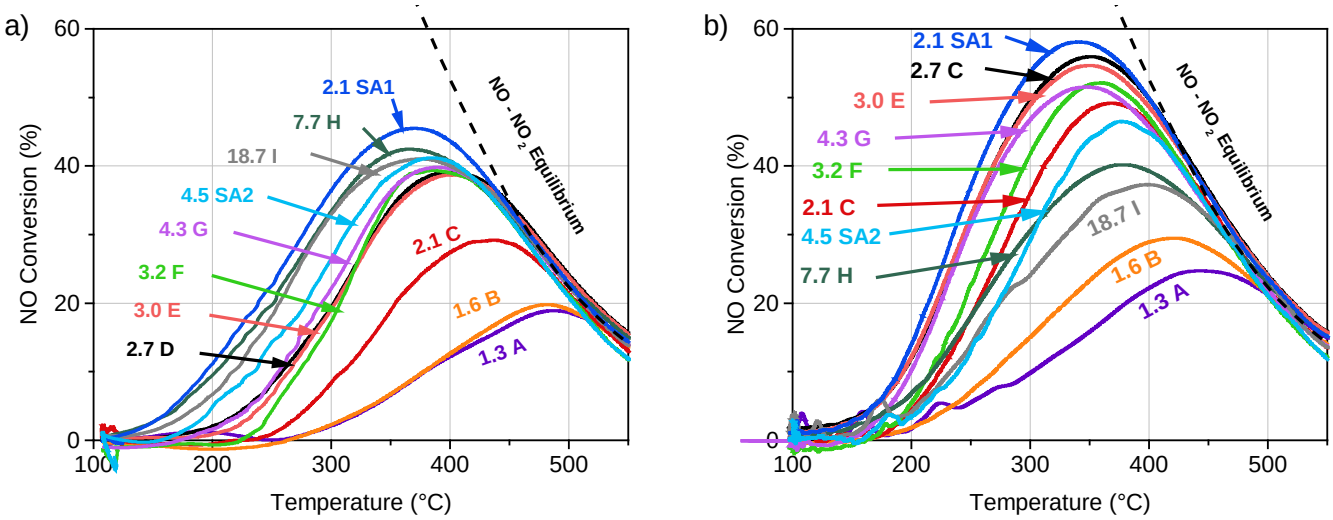
a)
NO Conversion (%)
Temperature (°C)
NO - NO2 Equilibrium
2.1 SA1
7.7 H
18.7 I
4.5 SA2
4.3 G
3.2 F
3.0 E
2.7 D
2.1 C
1.6 B
1.3 A
b)
NO Conversion (%)
Temperature (°C)
NO - NO2 Equilibrium
2.1 SA1
2.7 C
3.0 E
4.3 G
3.2 F
2.1 C
4.5 SA2
7.7 H
18.7 I
1.6 B
1.3 A

548 **Figure S4.**

549

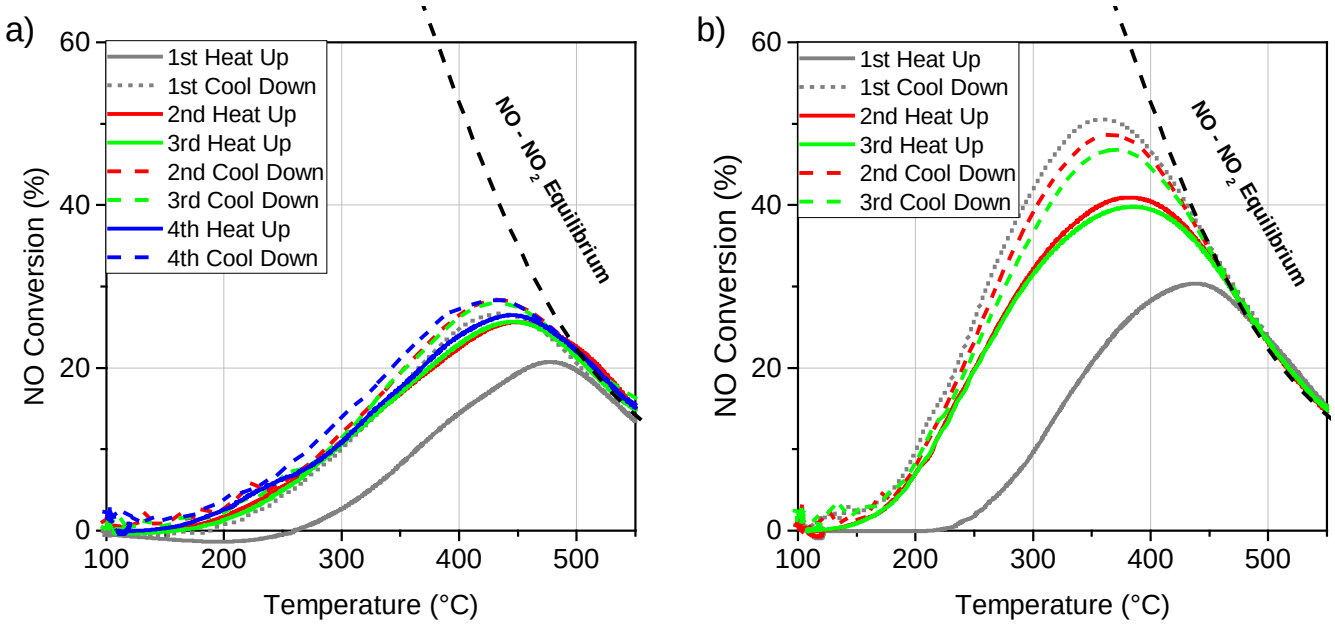

550